Originally Published at 2021 IEEE 23rd Electronics Packaging Technology Conference (EPTC)

Seeing beyond

Developments in Advanced Packaging Failure Analysis using Correlated X-ray Microscopy and LaserFIB

Vignesh Viswanathan, Longan Jiao, Cheryl Hartfield
Carl Zeiss Pte Ltd 80 Bendemeer Road, #10-01, Singapore 339949
vignesh.viswanathan@zeiss.com

Abstract

The evolution of packaging architecture with increasing density and scaling of features is resulting in large footprints to accommodate more components and functions that are integral in the heterogeneous integration roadmap and the More-than-Moore era. These developments pose new challenges in failure analysis and process characterization and drive need for advances in analysis tools, techniques, and development of novel workflows. In this work, we discuss the advances in two classes of techniques that have gained traction in the advanced packaging industry, 3D X-ray microscopy (XRM) and laser-integrated focused ion beam scanning electron microscopes (FIB-SEM) for sample preparation. While the laser integration in the FIB-SEM workflows has improved cross-section preparation throughput, precise targeting for site specific analysis of buried features requires the correlation with a complementary technique to provide sub-surface information. The use of 3D XRM to guide laser-integrated FIB-SEM analysis presents several advantages to address this challenge. In this work, we describe a novel workflow using 3D XRM and fs-laser integrated in a FIB-SEM (also called a LaserFIB) to precisely target and deliver results at high throughput. This represents a significant development in addressing the challenges of advanced package failure analysis.

Introduction

Advanced packaging developments for improved system performance and increased functionality in integrated circuits are driving the More-than-Moore era. Diverse 2.5/3D architectures with increasing density and shrinking interconnect dimensions and pitches, in combination with novel materials, has created complex challenges in package characterization and failure analysis (FA). These trends mandate new capabilities to enable fast development of package processes and rapid analysis of buried high density features. For physical analysis, non-destructive characterization at the micron scale using submicron 3D XRM for imaging and a LaserFIB for high throughput cross-section preparation and imaging has been explored previously and is becoming widely adopted [1-8]. X-ray computed tomography is an important non-destructive characterization technique in the package FA workflow. With the increasing footprints of over 100 x 100 mm^2 area and complex 2.5D and 3D architectures, submicron resolution for such large packages is challenging to achieve using conventional projection optics. The Resolution at a Distance (RaaD) capability and objective coupled scintillators in the ZEISS Xradia Versa X-ray microscope enables high-resolution imaging of large packages without compromising resolution [1-3]. With further developments in the recently introduced machine learning based reconstruction algorithms, improvements in both image quality and up to 4X increase in throughput can be achieved [9-11]. These improvements enable workflows using multiple 3D XRM scans to accurately localize defects and correlate with sample preparation techniques such as FIB-SEM.

Non-destructive analysis with 3D XRM is usually followed by physical analysis using mechanical or FIB cross-sections. Compared to the conventional Ga+ FIB, plasma FIB technology provides higher throughput for preparation of large cross-sections and volumes that are <0.5 mm^3 [12]. The addition of laser processing in the workflow has increased the throughput by multiple folds for larger volume removal and to access deeply buried structures using both standalone laser systems and integrated laser FIB systems as reported previously [4-8]. Adoption of pulsed femtosecond laser ablation results in a small laser-affected zone with minimal material damage even at high material removal rates. A parallel FIB-SEM and fs laser architecture enables laser milling in a separate chamber to promote cleanliness of the main FIB-SEM chamber for ultra high-resolution imaging and analysis. This integrated dual chamber architecture promotes ablation volumes as large as >10 mm^3 in lidded packages, stacked multi-dies and intact large packages.

To achieve high success rates in the failure analysis of site-specific buried defects, correlation with fault isolation techniques and 3D XRM is essential when preparing cross-sectional samples so that localized defects have the desired orientation for optimal viewing of the defect or process variations [12-14]. Here, the LaserFIB excels and offers higher precision and speed than standalone systems. Quick 3D XRM scans to verify the sample status at different stages of LaserFIB work promotes an ability to make adjustments to improve the targeting accuracy. To enable the workflow, precise registration of the coordinate systems between the X-ray tomography data and the LaserFIB is necessary to target subsurface sample features that are not visible by SEM or optical microscopy due to lack of fiducials or patterned features on the sample surface close to the region of interest. In this work, we address this challenge and present a novel 3D XRM and LaserFIB workflow that improves the laser targeting accuracy by using laser-patterned fiducial markers and Atlas 5 software to correlate 3D XRM and LaserFIB images, enabling precise buried feature targeting and high throughput LaserFIB sample preparation guided by 3D X-ray microscopy images.

Experimental Methods and Results

The workflow developed for precise targeting of sub-surface features is presented as a series of sequential steps in Figure 1.

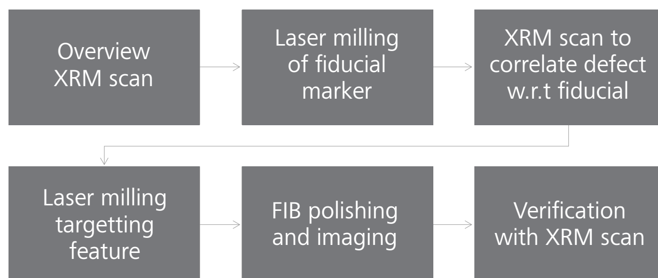

Figure 1 *Workflow overview.*

An overview XRM scan of the region of interest and high resolution scans, if required for visualization of the defect, are acquired. The sample surface near the deeply buried defect is then patterned with fiducial markers using the fs-laser. The sample is scanned again using the XRM to measure the relative position of the defect with respect to the fiducials on the sample surface. The coordinates mapping now provides the precise location for the laser milling pattern placement on the sample surface with respect to the fiducial markers for targeted sample preparation.

After the laser milling, the cross-section is further polished with the Ga FIB to remove the redeposition and small laser-affected zone, and to position the feature of interest in the desired final plane. The XRM tomography can be performed again at any point to verify the targeting accuracy.

The demonstration of this workflow is performed using ZEISS Xradia 520 Versa X-ray microscope and a ZEISS Crossbeam 350 laser FIB-SEM. The sample is an OLED display of a broken mobile phone. A small section at the top corner of the display, where the probability of defects is high, is cut and mounted on a pin for the XRM scan. For XRM-correlated LaserFIB work, the pin with the sample is mounted on a sample stub that mounts on the LaserFIB sample holder as shown in Figure 2b.

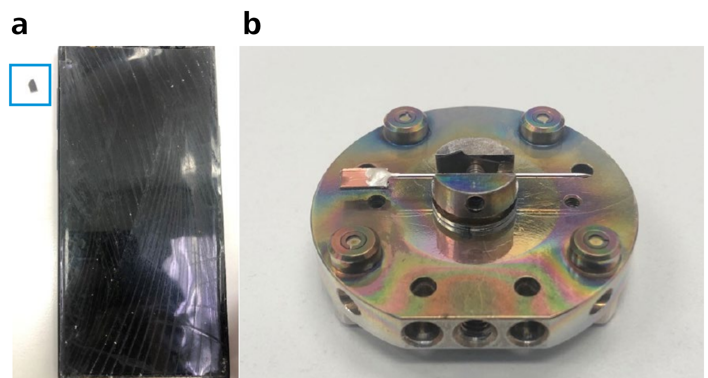

Figure 2 *(a) Small section of display from broken mobile phone is prepared and mounted on a pin for XRM investigation. (b) Pin is mounted on a stub on the LaserFIB sample holder to enable correlated LaserFIB processing.*

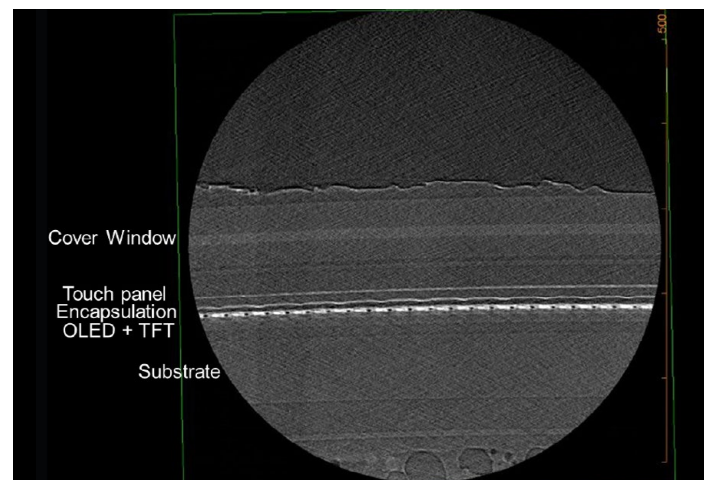

Figure 3 *XRM virtual cross-section of the OLED display with various layers highlighted. The strong absorption contrast in low Z materials allows clear identification of the different layers of polymeric and organic materials.*

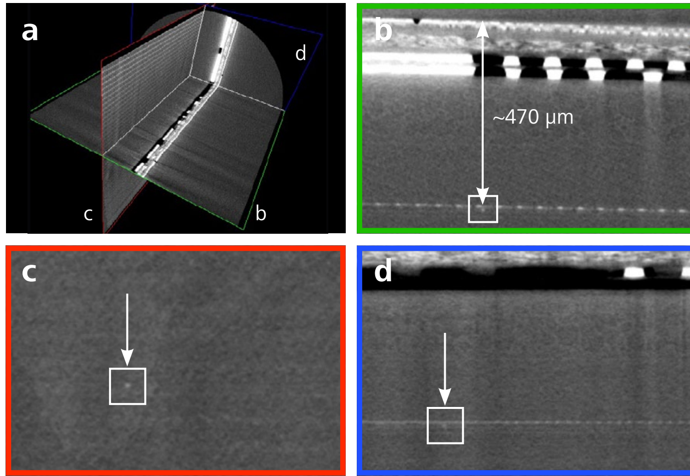

Figure 4 (a) 3D reconstructed volume highlighting the virtual cross sections in three orthogonal planes indicated by (b) green, (c) red and (d) blue. The defect particle is highlighted by the green, red and blue arrows in the respective planes.

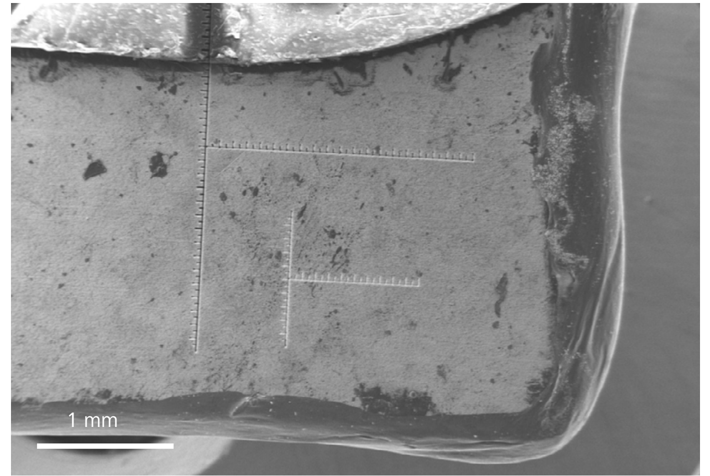

Figure 5 SEM image of the double ruler grid patterned using the fs laser with a major scale of 100 µm and minor scale of 50 µm over 1 mm x 1 mm for the smaller ruler and 2 mm x 2.7 mm for the larger ruler.

A low-resolution overview XRM scan of the sectioned sample is acquired in 2 hours with a resolution of 3 µm/voxel. The virtual cross-section shows the various layers in the display with good contrast of the organic and polymeric layers, indicating the mechanical sample preparation has caused minimum damage with most of the layers intact, Figure 3. Further analysis of the data indicates a particle defect is embedded inside a layer near the OLED and TFT circuitry, as seen in the virtual cross-sections at different planes as highlighted in Figure 4. The particle is estimated to be less than 10 µm in diameter and at a depth of 470 µm from the package substrate as indicated in Figure 4b. A higher resolution scan was not necessary since the particle is visible. However, there are no unique features to reference the position of the particle in the plane c shown in Figure 4c. Cross-section analysis of this defect particle requires an accurate determination of the particle position with reference to surface features near its location, enabling optimal placement of the FIB or laser milling patterns. Since the defect particle size is smaller than the 15 µm diameter of the fs-laser, the positioning information is critical.

To address these challenges, a fiducial marker that resembles a double grid is patterned on the surface of the sample using the ZEISS Crossbeam 350 laser FIB-SEM. The smaller grid is 1 mm x 1 mm long and larger grid is 2 mm x 2.7 mm. Both have a major spacing of 100 µm and minor spacing of 50 µm. The laser milling takes less than 10 seconds to pattern the fiducial, which can be customized to various grid spacings and orientations depending on the target feature. The pattern is immediately imaged with the electron column in the LaserFIB to check the laser milling fidelity and overall position of the marker, Figure 5. Optimization of the laser milling parameters for different or new materials can also be performed in this step to optimize the quality, calibrate milling rates, and achieve depth control.

Subsequently the sample is scanned with the XRM at the same region with the same parameters as the earlier scan. The 3D XRM data is imported into the LaserFIB's Atlas 5 software, and then using Atlas 5, 3D XRM virtual cross-sections at the plane of the defect are projected onto the plane with the fiducial markers to determine the position of the defect with respect to the grid, Figure 6.

With the defect coordinate locked-in relative to the marker grids, the milling patterns are positioned accordingly. The placement of the mill patterns position considers the 15 µm laser spot size and side wall taper created by the laser beam profile and is well calibrated to target the defect precisely.

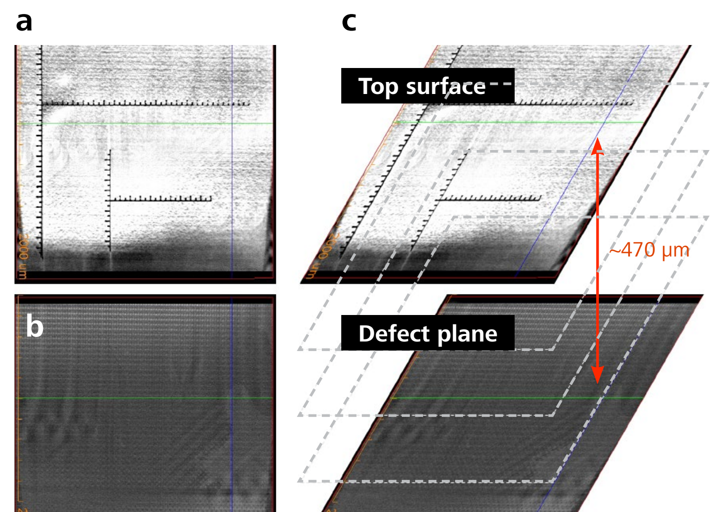

Figure 6 XRM virtual cross-section of the (a) top surface with fiducial markers and (b) defect with the position marked by the crosshair that is projected in the vertical plane to reference with the marker as shown in (c). The defect is ~470 µm below the surface and its position can be mapped to the grid.

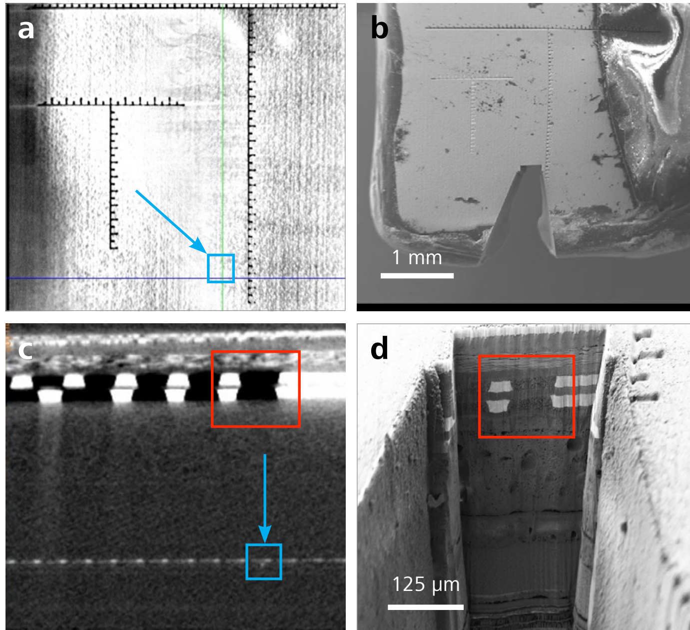

Figure 7 (a,c) XRM virtual cross-section with the arrow pointing to the position of the defect can be compared with the (b) top down and (d) cross-section SEM view of the laser milled patterns indicating accurate targeting of the defect particle. The metal layers in the substrate as highlighted by the box in (c, d) also provide a reference to the defect position.

The fs-laser milling is performed within 10 minutes in two steps: 1) a coarse laser mill at 15% of the maximum power to remove the bulk material, and 2) a fine laser mill at 8% power to polish the cross-section face and minimize damage to beam sensitive materials. The coarse mill volume with the trapezoid shape is about 0.85 mm^2 x 0.6 mm and the fine polish volume is 0.03 x 0.25 x 0.6 mm^3. Figure 7b shows the top-down view highlighting the position of the laser milled patterns with respect to the grid markers, and Figure 7d shows the cross-section view immediately after the laser milling. Comparing the XRM image in Figure 7a with the crosshairs highlighting the defect position, it can be observed that the laser milling is on target. The copper metal lines in the substrate can also provide an indication of the targeting accuracy as highlighted by the box in Figure 7c and d.

The particle is not clearly visible immediately after the laser milling due to redeposition and requires FIB polishing to clean up the surface. A gallium FIB polish at 65 nA for 20 minutes is performed to remove the redeposition and to target and expose the defective particle. The particle is visible immediately as the redeposition is cleared, although additional FIB polishing is required to remove the curtains and acquire a clear cross section. The final cross-section image with the in-column backscatter electron signal shows the defect in bright contrast indicating a metallic particle about 6.5 µm in diameter between the OLED and encapsulation layers, Figure 8.

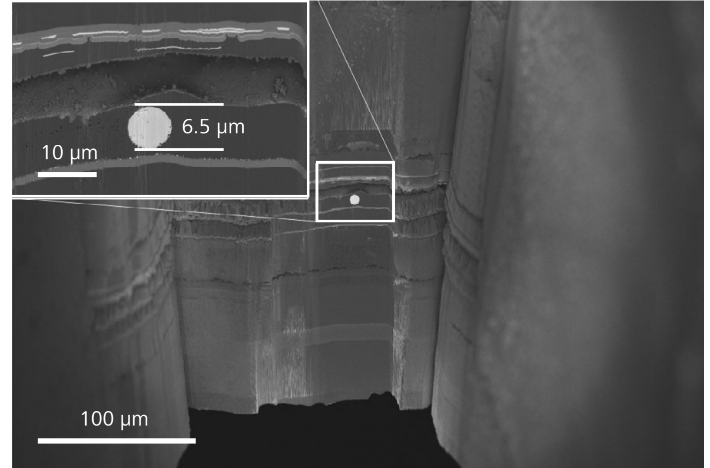

Figure 8 Cross-section image of the metallic defect with higher magnification inset with particle diameter measuring 6.5 µm.

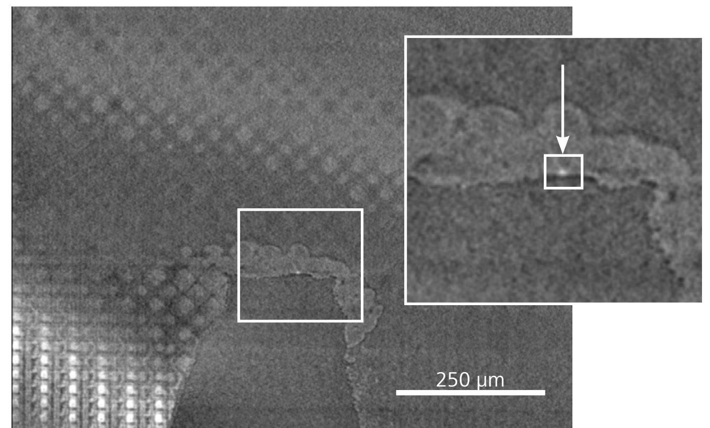

Figure 9 XRM virtual cross-section after laser and FIB milling indicating the particle was targeted precisely. The inset shows the particle highlighted by the arrow that is targeted in the preparation.

The targeting is verified with another XRM scan of the cross-sectioned sample. The virtual XRM cross section shows the particle cross-section perfectly aligned with the milled pattern, Figure 9.

Discussion

The workflow detailed in the earlier section demonstrates high precision in targeting deeply buried defects during failure analysis. The precision and minimum feature size that can be targeted is limited by two factors, the resolution of the X-ray microscope and the laser placement accuracy, which is on the order of 1-2 µm. In light of various fs-laser beam placement considerations including the laser spot size of <15 µm, the redeposition layer thickness, and the submicron laser affected zone, this work shows that this workflow for targeting deeply buried features of interest can routinely achieve laser targeting accuracy of better than 5 µm.

Continued developments to improve the laser accuracy will push the targeting accuracy towards the submicron scale, which further supports the requirements of 3D packaging technologies. However, additional understanding of the laser interactions with the new materials used in advanced packaging technologies would be necessary to achieve higher precision and targeting with this approach.

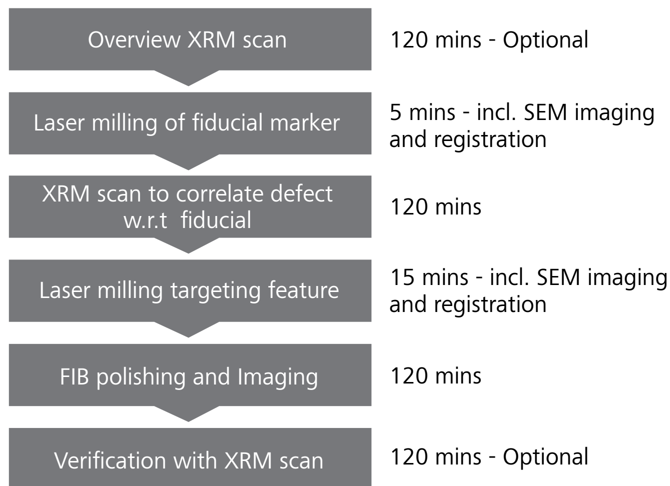

Figure 10 *Workflow overview with time taken for each step. Some of the 3D XRM steps are optional, depending on the fault isolation methods employed, which can significantly improve the time to result.*

Considering the throughput and time to result, we see that the workflow takes around 6:40 hours with the most time taken during the 3D XRM data acquisition, Figure 10. In most failure analysis, the fault isolation is performed using other techniques such as thermal emission, scanning acoustic microscopy, laser scanning confocal microscopy and other techniques. In such cases, step 1 in the workflow could be skipped to directly pattern the sample surface with the laser and execute 3D XRM scans to visualize the defect and correlate the fiducials on the surface. The final verification step with 3D XRM can also be omitted from the analysis in most cases. This lowers the time to results to about 2.5 hours in this case, which represents a significant improvement in both throughput and accuracy in site specific failure analysis of defects. Although there are multiple 3D XRM scans performed, the recently available advanced reconstruction techniques based on machine learning algorithms can significantly reduce the scan times while preserving the image quality to gain throughput in this workflow [10-11].

Conclusions

A novel correlative workflow using LaserFIB and 3D XRM techniques is presented for targeted cross-section preparation of deeply buried subsurface defects and features. The case study presented is a particle defect found in the OLED display from a used mobile phone. The 520 Versa 3D XRM was used to scan and identify the defect and correlate with surface features patterned on the sample using the Crossbeam 350 fs-Laser FIB-SEM for precise targeting and sample preparation. The large area cross sections were prepared using the fs-laser followed by Ga+ FIB polishing in 35 minutes. The particle size is 6.5 µm in diameter and buried about 470 µm from the package substrate surface close to the OLED and TFT layers. The entire process from defect isolation until the cross-section preparation and analysis of the defect is completed in less than 5 hours highlighting the throughput and precision capabilities of this streamlined workflow to meet the demands and success requirements in the failure analysis of advanced packages.

Acknowledgments

The authors would like to acknowledge the support from ZEISS Microscopy Customer Centre Shanghai in providing the microscopes and tools used to developthis workflow and would also like to thank Henry Cai for the samples donated for this case study.

References

1] Sylvester Y., Hunter L., Johnson B. and Estrada R., "3D X-ray microscopy: A near-SEM non-destructive imaging technology used in the development of 3D IC packaging," 2013 IEEE International 3D Systems Integration Conference (3DIC), 2013, pp. 1-7.

2] Zulkifli S. M., Zee B., Qiu W. and Gu A., "High-res 3D X-ray microscopy for non-destructive failure analysis of chip-to-chip micro-bump interconnects in stacked die packages," 2017 IEEE 24th International Symposium on the Physical and Failure Analysis of Integrated Circuits (IPFA), 2017, pp. 1-5.

3] Bhuvanendran Nair Gourikutty S., et al., "Defect Localization in Through-Si-Interposer Based 2.5D ICs," 2020 IEEE 70th Electronic Components and Technology Conference (ECTC), 2020, pp. 1180-1185.

4] Stegmann H., Dömer H., Cai H., Rosenkranz R. and Zschech E., "Efficient target preparation by combining laser ablation and FIB milling in a single tool," 2011 Semiconductor Conference Dresden, 2011, pp. 1-4.

5] Randolph, S. J., Filevich, J., Botman, A., Gannon, R., Rue, C., & Straw, M. "In situ femtosecond pulse laser ablation for large volume 3D analysis in scanning electron microscope systems" Journal of Vacuum Science & Technology B, Vol. 36, No. 6 (2018), 06JB01.

6] Tuček M., Blando R., Váňa R., Hladík L. and Oboňa J. V., "Speeding up large-scale failure analysis of semiconductor devices by laser ablation," 2020 IEEE International Symposium on the Physical and Failure Analysis of Integrated Circuits (IPFA), 2020, pp. 1-3.

7] Johnson G. M., Hartfield C., Mueller S. and Kaestner M., "New physical analysis capability for counterfeit electronics and reverse engineering," 2020 IEEE Physical Assurance and Inspection of Electronics (PAINE), 2020, pp. 1-5,

8] Tordoff B., Hartfield, C., Holwell, A.J. et al. "The LaserFIB: new application opportunities combining a high-performance FIB-SEM with femtosecond laser processing in an integrated second chamber," Appl. Microsc. Vol. 50, No. 24 (2020)

9] Andrew, M., and Hornberger, B. "Benchmarking of Machine Learning and Conventional Image Segmentation Techniques on 3D X-ray Microscopy Data". Microscopy and Microanalysis, 24(S2), (2018) pp.118-119

10] Gu A., Andreyev A., Terada M., Zee B., Zulfikli S.M. and Yang Y. "CASE STUDIES - DEVICE ANALYSIS: Accelerate Your 3D X-ray Failure Analysis by Deep Learning High Resolution Reconstruction", International Symposium for Testing and Failure Analysis (ISTFA), 2021

11] Andrew M., Sanapala R., Hartfield C. and Atkinson-Mora J. " Advanced Reconstruction Technologies for Semiconductor Advanced Packaging", Technical Note, https://zeiss.widen.net/s/7scxlhbhm8/en_wp_3d-xray-art-for-semiconductor

12] Hartfield C., Kaestner M., Mueller S., Atkinson-Mora J. and Schullmeyer I., "A new approach for rapid analysis of buried 2.5/3D package structures", Chip Scale Review Vol. 24, No. 3 (2020) pp. 39-42.

13] Kaestner M., Mueller S., Gregorich T., Hartfield C., Nolan C., Schulmeyer I., "Novel workflow for high-resolution imaging of structures in advanced 3D and fan-out packages", China Semiconductor Technology International Conference (CSTIC) (IEEE, Shanghai, 2019), pp. 1–3.

14] Leslie N., Lai B., Lee H., Lee M., Kang C.H., Patakova Z., Zelenka F., and Varslot T., "Addressing Failures in Advanced Packaging Through a Correlative Workflow" International Symposium for Testing and Failure Analysis (ISTFA), 2020, pp. 17-19.

microscopy@zeiss.com
www.zeiss.com/semiconductor-marketing